PHYSICAL REVIEW B VOLUME 32, NUMBER 5 1 SEPTEMBER 1985

Magnon-mass renormalization in $(CH_3)_4NMnCl_3$ (TMMC)

Nancy F. Wright and Michael D. Johnson
Department of Physics, University of Virginia, Charlottesville, Virginia 22901

Michael Fowler
Institute for Theoretical Physics, University of California at Santa Barbara, Santa Barbara, California 93106
and Department of Physics, University of Virginia, Charlottesville, Virginia 22901

(Received 25 March 1985)

If $(CH_3)_4NMnCl_3$ (TMMC) in a transverse magnetic field is represented by a quantum sine-Gordon Hamiltonian, the computed quantum renormalization of the classical soliton mass agrees well with experiment. However, the theory also predicts a substantial magnon-mass renormalization which is not observed. We compute the magnon-mass renormalization for the exact spin-chain Hamiltonian to the two-loop level, and show that, for the physical parameters appropriate to TMMC, the substantial sine-Gordon mass renormalization is largely cancelled by contributions from out-of-plane fluctuations not included in the sine-Gordon model. Our final result is in excellent agreement with recent experimental work.

I. INTRODUCTION

Much of the recent work on the magnetic properties of $(CH_3)_4NMnCl_3$ (TMMC) has been based on approximating it by a sine-Gordon system.[1-11] The generally accepted TMMC spin-chain Hamiltonian [given in Eq. (2.1) below] is a one-dimensional (1D) antiferromagnet of spins $\frac{5}{2}$, with an anisotropy term tending to keep the spins in an easy plane perpendicular to the line of magnetic ions.[12] In the classical ground state (thought to be a good starting point for TMMC in fields of a few tesla), the spins are in this easy plane, almost perpendicular to the applied external field. Elementary excitations are thought to consist of spin waves (magnons) and kinks. In the latter the spin direction twists through 180° while staying more or less in the easy plane. Thus, qualitatively, the spin chain has features in common with the sine-Gordon system. It has also been established, with certain approximations, that the spin-chain Hamiltonian can be transformed into the sine-Gordon Hamiltonian.[1,2] One of the important approximations is that each spin is nearly confined to the easy plane, even though for TMMC the measured value of the anisotropy parameter δ (which favors planar confinement) is quite small. Usually one argues that the strong nearest-neighbor coupling forces the spins to go out of the easy plane together, increasing the effectiveness of the anisotropy term.

Many properties of the quantum sine-Gordon system have been worked out using various field theoretic techniques, and recently some of these have been compared with experimental TMMC results.[4,5] The classical estimate of a bare kink or soliton mass is computed by assuming that the spins are classical, and by transforming the spin-chain Hamiltonian to a classical sine-Gordon equation. But, as pointed out by Maki,[4] quantum effects are actually quite important for TMMC. When they are included, the bare, or classical, soliton mass is renormalized downwards by about 40% (in a field of 5 T). This renormalization produces good agreement between theory and experiment. A similar result should hold true for the magnon mass: In the sine-Gordon theory of TMMC the magnon mass is renormalized downward by about 30% from its bare value $g\mu_B H$ (where H is the external magnetic field perpendicular to the chain).[4] Experimentally, however, only a small renormalization is observed.[13,14] In this paper we show that the application of field theoretic techniques directly to the spin-chain Hamiltonian yields a small mass renormalization very close to that experimentally observed; therefore, the sine-Gordon system is not in this respect an adequate representation of TMMC.

It should be noted, at this point, that in the absence of the easy plane anisotropy in the TMMC Hamiltonian (2.1) (i.e., for an isotropic Heisenberg antiferromagnetic chain in an external field), the spin waves have mass $g\mu_B H$, corresponding to the classical frequency. The Hamiltonian $\mathcal{H}=\mathcal{H}_0+\mathcal{H}_{\rm ext}$ commutes with the total spin component in the direction of the field, $S^x=\sum_n S_n^x$, so the energy of a zero momentum state is quantized in units of $g\mu_B H$: there is no quantum renormalization. When the easy plane anisotropy term $\mathcal{H}_\delta=\delta J\sum_n (S_n^z)^2$ is introduced, S^x is no longer a good quantum number and this argument fails. It might seem that a natural approach to the TMMC model (2.1) would be to do perturbation theory in the small term $\mathcal{H}_\delta$. Unfortunately, the ground state of the unperturbed system $\mathcal{H}=\mathcal{H}_0+\mathcal{H}_{\rm ext}$ is very complicated.

In this paper, following Riseborough and Reiter,[15] we take the classical easy plane antiferromagnetic state as the zeroth approximation, and expand in powers of the amplitude of the out-of-plane fluctuations $\langle (S_n^z)^2\rangle/[S(S+1)]$, and in-plane fluctuations $\langle(\Psi_n)^2\rangle$. This turns out to be the loop expansion of quantum field theory,[16] where, for a semiclassical spin, the leading term is the classical system, one-loop graphs are of order $\hbar$, two-loop graphs of order $\hbar^2$, and so on. More accurately, the graphs are of order

$1/S$, $1/S^2$, etc., and for a semiclassical system $\hbar S$ is of order unity. Because $S=\frac{5}{2}$ for TMMC, we adopt the latter description: graphs are of order $\{[S(S+1)]^{1/2}\}^{-1}$, $\{[S(S+1)]^{1/2}\}^{-2}$, etc. We carry out the expansion to the two-loop level, which involves computation of about 600 diagrams. Going beyond this order does not appear to be practical. We find, however, that the second-order correction is quite small (although it involves many cancellations among large terms), so we believe our approximation to be accurate.

An important feature of a loop expansion is that symmetries are preserved order by order. In particular, in the limit of δ going to zero, the magnon-mass renormalization disappears in each order (the dressed mass equals the bare mass) as discussed above. A difficulty is that some of the graphs diverge as δ goes to zero, so a good deal of care is needed in computing at small δ. Nevertheless, to first order the cancellation is readily apparent. Evaluation of the two-loop graphs is more challenging, but it is clear that the second-order renormalization from these graphs is also tending to zero with δ (at least until divergences render the numerical methods suspect). For TMMC the symmetry is only slightly broken (we find $\delta=0.019$ in Sec. V), and therefore the renormalization to each order should be small. This indeed turns out to be the case, as explained in Sec. V.

We have been able to compute the magnon-mass renormalization over a wide range of the anisotropy parameter δ and the external field H. For $\delta \ll H$ the spins precess about the external magnetic field. For $\delta \gg H$ the spins are confined to the x,y plane and behave in sine-Gordon fashion. We find that the spin-chain magnon-mass correction goes from zero to the sine-Gordon value (about 30% in a field of 5 T) as δ increases from zero to of order unity.

With these computations we are able to ascertain, for the first time, whether the actual δ for TMMC is large enough to enforce sine-Gordon behavior. We find this not to be the case. Nor is the assumption of Riseborough and Reiter[15]—that the in-plane graphs are dominant—valid for TMMC. Because of the large cancellation of in-plane by out-of-plane diagrams, we predict a mass renormalization for TMMC of 8% in a field of 5 T, so TMMC is much closer to the isotropic limit than to the sine-Gordon limit. What effect this out-of-plane motion has on soliton modes remains to be investigated.

It is assumed throughout this paper that the external field and anisotropy terms are sufficiently strong for the picture of magnon excitations from the ground state to be qualitatively valid. In particular, we assume that the external field is strong enough to suppress the (zero-field) nonlinear sigma excitations recently discussed by Haldane.[17]

We have used zero-temperature Green's functions throughout. Maki and Takayama have shown that in the sine-Gordon approximation, at temperatures comparable to those used in the experiments on TMMC, the magnon mass undergoes a further renormalization of a few percent.[18] However, the spin-chain renormalization is zero in the isotropic limit, as explained above, even at finite temperatures. For TMMC, in which the isotropic symmetry is only slightly broken, the spin-chain renormalization should vary with temperature even less than in the sine-Gordon approximation.

After this work had been submitted for publication, Dr. H. Shiba drew our attention to some recent experimental results[14] which are in very close agreement with the present analysis. In contrast to earlier work, the new experimental results are in clear disagreement with classical predictions. They agree well with the one-loop quantum corrections, as discussed by Shiba,[14] although the loop expansion is in powers of $1/S$, with $S=\frac{5}{2}$. We believe that an important feature of the present work is that, by using sine-Gordon type variables and symmetry arguments, it can be seen for the first time why higher-order terms in the series are much smaller than might be expected. We have been able to confirm this result numerically for the two-loop terms, which we find make only a tiny correction in the range of interest.

In Sec. II of this paper we review the derivation of the sine-Gordon Hamiltonian from the spin chain, and introduce some of the formalism used later. In Sec. III we give the sine-Gordon mass renormalization. Section IV describes the magnon-mass renormalization in the full spin-chain model to the two-loop level, and the results of the computation are presented in Sec. V.

II. THE SINE-GORDON APPROXIMATION

In this section we review the derivation of the sine-Gordon (SG) Hamiltonian from the generally accepted TMMC spin-chain (SC) Hamiltonian:[12]

$$\mathcal{H}=\mathcal{H}_0+\mathcal{H}_\delta+\mathcal{H}_{\rm ext}\,, \tag{2.1}$$

where

$$\mathcal{H}_0=J\sum_{n=1}^{N}\mathbf{S}_n\cdot\mathbf{S}_{n+1},\quad \mathcal{H}_\delta=\delta J\sum_{n=1}^{N}(S_n^z)^2\,,$$

$$\mathcal{H}_{\rm ext}=-g\mu_B H\sum_{n=1}^{N}S_n^x\,.$$

The SC is a line of spin vectors, one on each central Mn ion, with nearest-neighbor interactions. Each Mn ion has five valence electrons which, according to Hund's rules, half fill its d shell, giving $S=\frac{5}{2}$, $L=0$, and $g=2$. The large value of the ionic spin has prompted consideration of TMMC as a nearly classical system. The intrachain interaction, whose strength is of order JS^2, is much stronger than the interchain interaction, $J'S^2$, as a result of the physical separation imposed by the large $(CH_3)_4N^+$ complexes. Since TMMC has a ratio J/J' of roughly 1000, it has essentially 1D behavior above the three-dimensional ordering temperature T_N. (T_N is a function of field, varying from 0.84 K at $H=0$ to approximately 3 K at $H=8$ T.[7]) The spin-chain parameter J is large and positive (antiferromagnetic) and δ is rather small. Currently accepted values for these parameters are $J/k_B=13.4$ K and $\delta=0.016$.[19] (As a result of our improved SC calculation, we determine the best fit to be $J/k_B=13.1$ K and $\delta=0.019$.) As explained in the Introduction, the mass renormalization varies slowly with temperature near the isotropic limit; therefore, the use of zero-temperature

Green's functions should be accurate over the experimental temperature range.

The following simple picture of TMMC dynamics in a transverse field has led to the belief that a sine-Gordon picture might be reasonable. For a chain along the $\hat{z}$ axis, with a magnetic field along the $\hat{x}$ axis, the classical ground-state spins on the even- (odd-) site sublattice are almost along the $+$ $(-)$ $\hat{y}$ axis. Each spin is in fact slightly canted in the direction of the field through a small angle α ($\alpha \sim H/4JS$). For the $T \ll JS^2/k_B$ dynamics, the short-range antiferromagnetic ordering is preserved, and for low enough temperatures, most of the spins will be approximately in the $\pm\hat{y}$ direction. However, there will be thermally generated magnons and kinks or solitons, where the local antiferromagnetic order turns through π (like a twist in a ribbon) as one moves along the chain. Assuming the spins stay in the easy plane, this is sine-Gordon-like behavior. For TMMC the small value of δ casts some doubt on the validity of the sine-Gordon representation from the beginning. However, as mentioned above, it has been argued that for the temperature range of interest ($T \ll JS^2/k_B$) the large value of J forces spins leaving the easy-magnetization plane to take others with them (of the order of the number of spins in a coherence length). Moving a number of spins out of the easy-magnetization plane would increase the energy cost, thereby enhancing the effect of the anisotropy term δ.

We now present a formal derivation of the sine-Gordon equation from the spin-chain Hamiltonian (2.1). The natural variables for an easy x,y-plane system are ϕ and S^z, where ϕ is the angular variable in the x,y plane defined by

$$S^{\pm}=(S\pm S_n^z)^{1/2}e^{\pm i\phi_n}(S\mp S_n^z)^{1/2} \tag{2.2}$$

and

$$F(S_n^z)e^{\pm i\phi_n}=e^{\pm i\phi_n}F(S_n^z\pm 1)\ . \tag{2.3}$$

The transformation (2.2) is used by Haldane,[17] and is equivalent to that used by Riseborough and Reiter,[15] except for the commutation relation (2.3), as explained below. [In addition, the form (2.2) establishes the proper ordering of the operators S_n^z and ϕ_n at the outset.] From (2.2) and (2.3) we find, following Haldane,

$$S_n^x=\sqrt{S(S+1)}\sum_m \alpha_m\left[\frac{S_n^z}{\sqrt{S(S+1)}}\right]^m\cos(\phi_n)\times\left[\frac{S_n^z}{\sqrt{S(S+1)}}\right]^m, \tag{2.4}$$

where

$$\sum_m \alpha_m x^m=\sqrt{1-x}\ . \tag{2.5}$$

Note that the mth term of this expansion is of order $(S^z/S)^{2m}$, so that physical properties computed using this series should converge rapidly if the system stays close to the easy-magnetization plane. Substitution of the series (2.4) and the more complicated

$$\tfrac{1}{2}(S_n^+S_{n+1}^-+S_n^-S_{n+1}^+)=S(S+1)\left[\cos(\phi_n-\phi_{n+1})-\frac{1}{2}\frac{S_n^z}{\sqrt{S(S+1)}}\cos(\phi_n-\phi_{n+1})\frac{S_n^z}{\sqrt{S(S+1)}}-\frac{1}{2}\frac{S_{n+1}^z}{\sqrt{S(S+1)}}\cos(\phi_n-\phi_{n+1})\frac{S_{n+1}^z}{\sqrt{S(S+1)}}+\cdots\right] \tag{2.6}$$

into the Hamiltonian (2.1), and expanding to second order in $S^z/\sqrt{S(S+1)}$, gives[15]

$$\mathcal{H}=JS(S+1)\sum_{n=1}^{N}\left[\cos(\phi_n-\phi_{n+1})-\frac{g\mu_BH}{J\sqrt{S(S+1)}}\cos(\phi_n)+\frac{S_n^zS_{n+1}^z}{S(S+1)}-\frac{1}{2}\frac{S_n^z}{\sqrt{S(S+1)}}\left[\cos(\phi_n-\phi_{n+1})+\cos(\phi_{n-1}-\phi_n)-\frac{g\mu_BH}{J\sqrt{S(S+1)}}\cos(\phi_n)-2\delta\right]\frac{S_n^z}{\sqrt{S(S+1)}}\right]. \tag{2.7}$$

(In Appendix A we continue this expansion to order $[S^z/\sqrt{S(S+1)}]^6$, necessary for Sec. IV.)

We assume that the local quantum fluctuations in ϕ are small enough ($\ll 2\pi$), to allow us to neglect its angular nature and treat ϕ_n, S_n^z as conjugate variables.[20] Rather than the commutation (2.3) (true for action-angle variables), we take

$$[\phi_n,S_n^z]=i\ . \tag{2.8}$$

Next we transform variables from ϕ_n to Ψ_n using[15]

$$\phi_n=(-1)^n(\pi/2-\alpha)+\Psi_n\ , \tag{2.9}$$

where α is the canting angle, and thus Ψ_n is the planar angle measured from the classical ground-state position of the spins. The canting angle α is found by minimizing the ground-state energy

$$E_{GS}=-JS(S+1)N\left[\cos(2\alpha)+\frac{g\mu_BH}{J\sqrt{S(S+1)}}\sin(\alpha)\right], \tag{2.10}$$

giving

$$\sin\alpha=\frac{g\mu_BH}{4J\sqrt{S(S+1)}}\ . \tag{2.11}$$

This choice of α [equal to the classical canting angle except for the replacement of S by $\sqrt{S(S+1)}$] eliminates the linear term in the Hamiltonian which results from the substitution (2.9). The expansion based on (2.9) will be used in Sec. IV.

For the purposes of this section, we will use a modification of (2.9). In general, the canting angle depends on the field strength perpendicular to the spins (changing as the spins twist around to form, say, a soliton). To allow for large fluctuations, a more natural transformation for ϕ_n would be

$$\phi_n=(-1)^n[\pi/2-\alpha\cos(\Psi_n)]+\Psi_n \ . \tag{2.12}$$

Substituting (2.12) into (2.7), subtracting off the ground-state energy, and dropping terms higher than second order in the small parameters α, $\Psi_n-\Psi_{n+1}$, and $S_n^z/\sqrt{S(S+1)}$, we find

$$\mathscr{H}=JS(S+1)\sum_{n=1}^{N}\left[\alpha^2[1-\cos(2\Psi_n)]+\tfrac{1}{2}(\Psi_n-\Psi_{n+1})^2+(2+\delta)\frac{(S_n^z)^2}{S(S+1)}\right] . \tag{2.13}$$

In (2.12) the canting angle, $\alpha\cos(\Psi_n)$, becomes a dynamical variable, so that (2.8) no longer implies $[\Psi_n,S_n^z]=i$. The extra terms in the commutator are smaller by order α, however, and can be neglected. To leading order, then, (2.13) gives

$$\frac{d}{dt}(\Psi_n)=\frac{2J(2+\delta)}{\hbar}S_n^z \ . \tag{2.14}$$

We define

$$\Theta_n=\frac{2}{g}\Psi_n \tag{2.15}$$

to give the conventional sine-Gordon angular variable which undergoes a $2\pi/g$ rotation between successive ground states, where g^2, the dimensionless coupling constant, is proportional to the ratio of the magnon mass to the classical soliton mass. With these substitutions, and in the continuum limit, (2.13) becomes

$$\mathscr{H}_{\rm SG}=\tfrac{1}{2}Ag^2\int dx\left[(\Theta_t)^2+c^2(\Theta_x)^2+\frac{2(\omega_0^*)^2}{g^2}[1-\cos(g\Theta)]\right] , \tag{2.16}$$

where

$$A=\frac{\hbar^2}{16J(1+\delta/2)a} \ , \tag{2.17}$$

$$\hbar c=2Ja\sqrt{S(S+1)}\sqrt{1+\delta/2} \ , \tag{2.18}$$

$$\hbar\omega_0^*=g\mu_B H\sqrt{1+\delta/2} \ , \tag{2.19}$$

a equals the spacing between Mn ions, and g^2 is chosen so that

$$Ag^2=\hbar/c \ . \tag{2.20}$$

For the antiferromagnetic spin chain,

$$g^2=8\left[\frac{1+\delta/2}{S(S+1)}\right]^{1/2} . \tag{2.21}$$

In comparing our expressions with the literature, note that sometimes $2J$ is used in place of J in the Hamiltonian (2.1). In our notation, a is the Mn-Mn spacing, not the classical antiferromagnetic sublattice unit-cell size, which we write as $2a$. Finally, note that $\sqrt{S(S+1)}$ occurs in place of S because of the transformation (2.2) used to expand the Hamiltonian. The difference is significant for TMMC, where $S=\frac{5}{2}$.

III. SINE-GORDON MAGNON-MASS RENORMALIZATION

The computation of the mass renormalization for the sine-Gordon Hamiltonian is a standard quantum field theoretic exercise.[18,21] Here we briefly recapitulate the argument and the results.

One expands the $2(\omega_0^*)^2[1-\cos(g\Theta)]/g^2$ term in (2.16) to obtain the mass term, $(\omega_0^*)^2\Theta^2$, and an infinite series of higher-order interactions $-g^2\Theta^4/4!$, $g^4\Theta^6/6!$, etc. Diagonalizing the quadratic terms gives the bare (classical) magnon dispersion relation; the higher-order terms renormalize this energy. It is well known that the logarithmically divergent contributions (as the momentum cutoff $\Lambda\to\infty$) to the dressed mass can be eliminated by simply normal ordering the Hamiltonian (2.16).[21] The result is that the bare mass m^* (given by $\hbar\omega_0^*/c^2$) is replaced by a dressed mass m, where, at $T=0$,

$$m=m^*\exp(-\tfrac{1}{4}g^2D) \tag{3.1}$$

and

$$D=\langle\Theta^2\rangle=\frac{1}{4\pi}\int_{-\Lambda}^{\Lambda}dp\frac{1}{(m^2c^2+p^2)^{1/2}}=\frac{1}{2\pi}\ln(2\Lambda/mc) \ . \tag{3.2}$$

Graphically this renormalization represents the series of terms depicted in Fig. 1, where the dressed propagator is used self-consistently in the loops. The underlying lattice structure imposes a momentum cutoff $\Lambda=\pi\hbar/a$.

Solving for the dressed mass in terms of the bare propagator, we find

$$m=m^*\exp(-\tfrac{1}{4}\hat{g}^2D^*) \ , \tag{3.3}$$

where

$$\hat{g}^2=\frac{g^2}{1-g^2/8\pi} \tag{3.4}$$

and

$$D^*=\frac{1}{2\pi}\ln(2\Lambda/m^*c)=\frac{1}{2\pi}\ln(\pi/\alpha) \ . \tag{3.5}$$

In the next section we shall compute the magnon-mass renormalization to two loops using the spin-chain Hamiltonian, without the simplifying SG approximations. For comparison, we compute the SG renormalization to two loops, including the diagram not divergent with Λ, for the discrete form of (2.16). The appropriate diagrams are shown in Fig. 2.

Using the zero-temperature Green's function, the renormalized mass m (to two loops) is the solution of

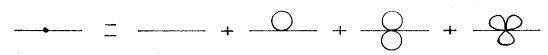

FIG. 1. Series of logarithmically divergent diagrams equivalent to normal ordering the sine-Gordon Hamiltonian. The dressed propagator is used self-consistently in the loops.

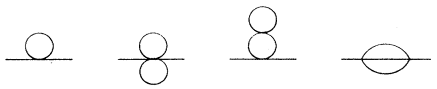

FIG. 2. One- and two-loop SG diagrams. Bare propagators are used to obtain correspondence with the SC results.

$$m^2=(m^*)^2(1+\theta^{(1)}+\theta^{(2)}) , \tag{3.6}$$

where the one- and two-loop corrections are, respectively,

$$\theta^{(1)}=-\tfrac{1}{2}g^2D^* \tag{3.7}$$

and

$$\theta^{(2)}=\tfrac{1}{8}g^4(D^*)^2-\frac{1}{16\pi}g^4D^*+F_{44} . \tag{3.8}$$

F_{44}, the contribution from the ω-dependent graph of Fig. 2, is given by

$$F_{44}=-4\hbar\omega_0^*\alpha^2\frac{1}{(2\pi)^2}\int_{-\pi}^{\pi}dq_1\int_{-\pi}^{\pi}dq_2\int_{-\pi}^{\pi}dq_3\,\delta(q_1+q_2+q_3)\alpha_{q_1}^2\alpha_{q_2}^2\alpha_{q_3}^2\frac{\omega_{q_1}+\omega_{q_2}+\omega_{q_3}}{(\omega_{q_1}+\omega_{q_2}+\omega_{q_3})^2-\omega^2-i\epsilon} , \tag{3.9}$$

where

$$\alpha_q^2=\langle\Theta_q\Theta_{-q}\rangle=\frac{1}{2\omega_q^2}(c/a) ,$$
$$\hbar\omega_q=4J\sqrt{S(S+1)}\sqrt{1+\delta/2}[\alpha^2+\sin^2(q/2)]^{1/2} . \tag{3.10}$$

To order g^2 (i.e., to order $[S(S+1)]^{-1}$), the mass is given by

$$m=m^*[1+\tfrac{1}{2}\theta^{(1)}+\tfrac{1}{2}\theta^{(2)}-\tfrac{1}{8}(\theta^{(1)})^2] . \tag{3.11}$$

IV. MAGNON-MASS RENORMALIZATION IN THE SPIN-CHAIN MODEL

In this section we investigate the magnon-mass renormalization directly using the TMMC spin-chain Hamiltonian (2.1), going to the two-loop level. In contrast with the sine-Gordon field theory, in SC diagrams the vertices are momentum dependent, and the lines can be formed from any of four different propagators. The multiplicity of diagrams and their greater complexity make it impractical to go beyond two loops. Nevertheless, we believe the calculation is accurate for two reasons. In the SG approximation, discussed above, the mass renormalization including only "divergent" graphs through two loops [setting $F_{44}=0$ in (3.8)] gives an answer within 1% of the infinite-order mass (3.3), for fields of 2 to 8 T. Moreover, in TMMC the isotropic symmetry is barely broken, suppressing the renormalization from each order. In the SC analysis the second-order correction (two-loop graphs plus the second-order contribution from one-loop graphs) adds from 0.2% to 2% to the one-loop renormalization, which for corresponding fields ranges from 5% to 15%.

We find, as previously mentioned, that the rather large magnon-mass renormalization predicted by sine-Gordon theory (but not observed experimentally in TMMC) does not occur in the SC calculation. The difference is explained by the inclusion of significant out-of-plane terms neglected in the SG approximation.

The change of variables (2.2) and (2.9) yields the quadratic Hamiltonian

$$\mathcal{H}_0=JS(S+1)\sum_n\left[\Psi_n\Psi_n-\cos(2\alpha)\Psi_n\Psi_{n+1}+\left[1+\frac{\delta}{2}\right]\frac{S_n^zS_n^z}{S(S+1)}+\frac{S_n^zS_{n+1}^z}{S(S+1)}\right] \tag{4.1}$$

and the interaction terms shown in Appendix A.[15] Transforming to momentum space,

$$\Psi_n=\frac{1}{\sqrt{N}}\sum_q e^{iqn}\Psi_q ,$$
$$S_n^z=\frac{1}{\sqrt{N}}\sum_q e^{iqn}S_q^z , \tag{4.2}$$

where $q\,(=ka)\in[-\pi,\pi]$, Eq. (4.1) becomes

$$\mathcal{H}_0=JS(S+1)\sum_q\left[\Psi_q\Psi_{-q}[1-\cos(2\alpha)\cos(q)]+\frac{S_q^zS_{-q}^z}{S(S+1)}[1+\delta+\cos(q)]\right] . \tag{4.3}$$

This is diagonalized by the Bogoliubov transformation:

$$\Psi_q=\alpha_q(a_q^\dagger+a_{-q}) ,$$
$$S_q^z=i\beta_q(a_q^\dagger-a_{-q}) , \tag{4.4}$$

where $\alpha_q\beta_q=\frac{1}{2}$ preserves the canonical commutation relations in Ψ_n and S_n^z. We find[15]

$$\alpha_q=\left[\frac{1}{4S(S+1)}\frac{1+\delta+\cos(q)}{1-\cos(2\alpha)\cos(q)}\right]^{1/4} ,$$
$$\beta_q=\left[\frac{S(S+1)}{4}\frac{1-\cos(2\alpha)\cos(q)}{1+\delta+\cos(q)}\right]^{1/4} , \tag{4.5}$$

and

$$\mathcal{H}_0=\sum_q\hbar\omega_q(a_q^\dagger a_q+\tfrac{1}{2}) , \tag{4.6}$$

where

$$\hbar\omega_q = 2J\sqrt{S(S+1)} \times\sqrt{[1+\delta+\cos(q)][1-\cos(2\alpha)\cos(q)]} \ . \quad (4.7)$$

Osano, Shiba, and Endoh[19] obtain a slightly different result because their expansion is in S^{-1}, rather than $[S(S+1)]^{-1/2}$. Also, their division of the system into sublattices splits our $[0,\pi]$ range into two ranges: $[0,\pi/2]$, which gives their α magnon; and the range $[\pi/2,\pi]$ (mapped into $[0,\pi/2]$, which gives their β magnon.

The transformed Hamiltonian, written to sixth order in Appendix A, exhibits the momentum dependence which complicates the SC diagrammatic analysis. A greater complication is the fact that the magnon-magnon interaction terms are functions of both Ψ and S^z, unlike the sine-Gordon case which has only the single operator θ. We treat Ψ and S^z on an equal footing by using a matrix form of the (phonon-type) zero-temperature Green's function:

$$\underline{D} = \begin{bmatrix} D_{\Psi\Psi} & D_{\Psi S} \\ D_{S\Psi} & D_{SS} \end{bmatrix} , \quad (4.8)$$

where

$$D_{\mu\nu}(q,t-t') = -i\langle T[\Phi^{\mu}_{q}(t)\Phi^{\nu}_{-q}(t')]\rangle \ , \quad \mu,\nu=\Psi \text{ or } S, \ \Phi^{\Psi}_{q}=\Psi_q, \ \Phi^{S}_{q}=S^z_q \ . \quad (4.9)$$

In terms of α_q, β_q, and ω_q [Eqs. (4.5) and (4.7)], the bare propagators are given (after Fourier transformation) by

$$\underline{D}^0(p,\omega) = \begin{bmatrix} 2\alpha_p^2\omega_p & i\omega \\ -i\omega & 2\beta_p^2\omega_p \end{bmatrix} \frac{1}{\omega^2-\omega_p^2+i\epsilon} \ . \quad (4.10)$$

We represent the bare propagators graphically by the four lines shown in Fig. 3. The Green's function for the interacting system obeys a matrix form of Dyson's equation (see Appendix B), and can be written

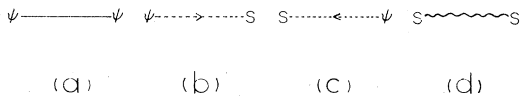

FIG. 3. Diagrammatic representation of bare SC propagators: (a) $D^0_{\Psi\Psi}$, (b) $D^0_{\Psi S}$, (c) $D^0_{S\Psi}$, (d) D^0_{SS}.

$$\underline{D}(p,\omega) = \begin{bmatrix} 2\alpha_p^2\omega_p(1+\theta_{ss}) & i\omega(1+\theta_{\Psi S}) \\ -i\omega(1+\theta_{\Psi S}) & 2\beta_p^2\omega_p(1+\theta_{\Psi\Psi}) \end{bmatrix} \times[\omega^2(1+\theta_{\Psi S})^2-(\omega_p-i\epsilon)^2(1+\theta_{\Psi\Psi}) \times(1+\theta_{SS})]^{-1} \ , \quad (4.11)$$

where

$$\theta_{\Psi\Psi}=\frac{2\alpha_p^2}{\omega_p}\Sigma_{\Psi\Psi}(p,\omega), \quad \theta_{SS}=\frac{2\beta_p^2}{\omega_p}\Sigma_{SS}(p,\omega) \ ,$$
$$\theta_{\Psi S}=\frac{i}{\omega}\Sigma_{\Psi S}(p,\omega) \ , \quad (4.12)$$

and the $\Sigma_{\mu\nu}$ are elements of a self-energy matrix. The dressed magnon energies are given by the poles of the propagator function (4.11), where, in the two-loop calculation, we keep only terms up to order $[S(S+1)]^{-1}$ [cf. Eq. (4.19)]. For comparison with the SG, we distinguish between in-plane graphs (those depending only on Ψ and therefore contributing only to $\Sigma_{\Psi\Psi}$) and out-of-plane graphs [which include powers of $S^z/\sqrt{S(S+1)}$].

The remaining task is the computation of the self-energy (irreducible connected) graphs which sum to give the Σ functions. To show the procedures involved, we summarize the calculation of a few of the simplest graphs. Diagrams are terms in the Wick's expansion of the usual perturbation series in the interaction Hamiltonian $\mathscr{H}'$:[22]

$$D_{\mu\nu}(p,t-t') = \sum_{n=0}^{\infty}\frac{(-i)^{n+1}}{n!}\int_{-\infty}^{\infty}dt_1\int_{-\infty}^{\infty}dt_2\cdots\int_{-\infty}^{\infty}dt_n\langle T[\Phi^{\mu}_{p}(t)\Phi^{\nu}_{-p}(t')\mathscr{H}'(t_1)\mathscr{H}'(t_2)\cdots\mathscr{H}'(t_n)]\rangle_{\text{conn}} \ . \quad (4.13)$$

$\Sigma_{\mu\nu}$ is the sum of the self-energy parts of all irreducible diagrams with input (output) operators Φ^{μ} (Φ^{ν}) (as explained in Appendix B).

Consider the simplest graphs, the $n=1$ contributions of $\mathscr{H}_4$ to $D_{\Psi\Psi}$. From (A6), $\mathscr{H}_4$ is itself the sum of three terms:

$$\mathscr{H}_4=\mathscr{H}^{\mathrm{a}}_4+\mathscr{H}^{\mathrm{b}}_4+\mathscr{H}^{\mathrm{c}}_4 \ ,$$
$$\mathscr{H}^{\mathrm{a}}_4=\sum_{q_1,q_2,q_3,q_4}V^{\mathrm{a}}(\mathbf{q})\Psi_{q_1}\Psi_{q_2}\Psi_{q_3}\Psi_{q_4} \ ,$$
$$\mathscr{H}^{\mathrm{b}}_4=\sum_{q_1,q_2,q_3,q_4}V^{\mathrm{b}}(\mathbf{q})S^z_{q_1}\Psi_{q_2}\Psi_{q_3}S^z_{q_4} \ , \quad (4.14)$$
$$\mathscr{H}^{\mathrm{c}}_4=\sum_{q_1,q_2,q_3,q_4}V^{\mathrm{c}}(\mathbf{q})S^z_{q_1}S^z_{q_2}S^z_{q_3}S^z_{q_4} \ .$$

The $n=1$ contributions of $\mathscr{H}_4$ to $D_{\Psi\Psi}$ are shown graphically in Fig. 4. $\mathscr{H}^{\mathrm{a}}_4$ contributes only to $\Sigma_{\Psi\Psi}$, $\mathscr{H}^{\mathrm{c}}_4$ only to Σ_{SS}, and $\mathscr{H}^{\mathrm{b}}_4$ contributes to all of $\Sigma_{\Psi\Psi}$, Σ_{SS}, $\Sigma_{\Psi S}$, and $\Sigma_{S\Psi}$ (although the latter two terms vanish in this case). The diagrams in Figs. 4(b) and 4(d) are the connected graphs in the Wick's expansion of

$$D^{4\mathrm{b}}_{\Psi\Psi}(p,t-t') = (-i)^2\int_{-\infty}^{\infty}dt_1\langle T[\Psi_p(t)\Psi_{-p}(t')\mathscr{H}^{\mathrm{b}}_4(t_1)]\rangle_{\text{conn}} \ , \quad (4.15)$$

which we write (after Fourier transformation) as

$$D^{(4\mathrm{b})}_{\Psi\Psi}(p,\omega)=D^0_{\Psi\Psi}\Sigma^{(4\mathrm{b})}_{\Psi\Psi}D^0_{\Psi\Psi}+D^0_{\Psi S}\Sigma^{(4\mathrm{b})}_{SS}D^0_{S\Psi} +D^0_{\Psi\Psi}\Sigma^{(4\mathrm{b})}_{\Psi S}D^0_{S\Psi}+D^0_{\Psi S}\Sigma^{(4\mathrm{b})}_{S\Psi}D^0_{\Psi\Psi} \ , \quad (4.16)$$

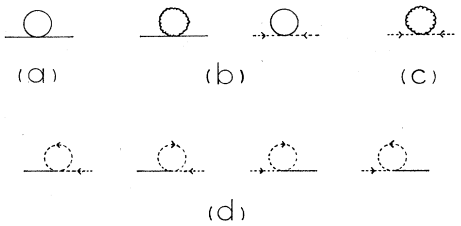

FIG. 4. The $n=1$ contributions of $\mathscr{H}_4$ to $D_{\Psi\Psi}$ [see Eq. (4.13)]: (a) $\mathscr{H}_4^a$, (b) $\mathscr{H}_4^b$, (c) $\mathscr{H}_4^c$, (d) graphs from $\mathscr{H}_4^b$ which cancel.

where

$$\Sigma_{\Psi\Psi}^{(4b)}(p,\omega)=-\frac{J}{\pi}\int_{-\pi}^{\pi}\beta_q^2[\sin^2(\alpha)+2\cos(2\alpha)\sin^2(p/2)]dq\ ,$$

$$\Sigma_{SS}^{(4b)}(p,\omega)=-\frac{J}{\pi}\int_{-\pi}^{\pi}\alpha_q^2[\sin^2(\alpha)+2\cos(2\alpha)\sin^2(q/2)]dq\ , \tag{4.17}$$

$$\Sigma_{\Psi S}^{(4b)}=\Sigma_{S\Psi}^{(4b)}=0\ .$$

Note that the computation of the self-energy terms (4.17) is greatly simplified by the symmetry of $V^b(\mathbf{q})$ under the exchange of q_1 and q_4, or of q_2 and q_3 [i.e., exchanges of indices within the set of S_q^z or Ψ_q operators separately; see (4.14) and (A6)]. As a result, terms in the Wick's expansion of (4.13) which differ by permutations of the Ψ_q's or S_q^z's give the same result—a nontrivial simplification since the vertices are momentum dependent. We have written the entire expansion of $\mathscr{H}'$ in Appendix A to take advantage of such symmetries. Appendix C shows several more examples.

The number of loops in a diagram is

$$L=I-(N-1)\ , \tag{4.18}$$

where I is the number of internal lines and N is the number of vertices. The number of loops equals the order of the diagram in the expansion parameter $[\sqrt{S(S+1)}]^{-1}$, which, in the semiclassical limit, is equivalent to the usual loop expansion in $\hbar$ of quantum field theory.[16] Figure 5 shows the one- and two-loop in-plane graphs for the SC expansion. Each of these in-plane diagrams represents a family of graphs in which the lines are replaced by out-of-plane propagators (as in Fig. 4). The three one-loop families represent 15 graphs, and the 23 two-loop diagrams represent 582 graphs. The contributions of the 597 graphs are summed to give the $\theta_{\mu\nu}$ in Eq. (4.12).

To compute the magnon-mass renormalization consistently to second order, in the two-loop computation we expand the square-root expression for the poles of the Green's function (4.11), keeping terms only to $[S(S+1)]^{-1}$:

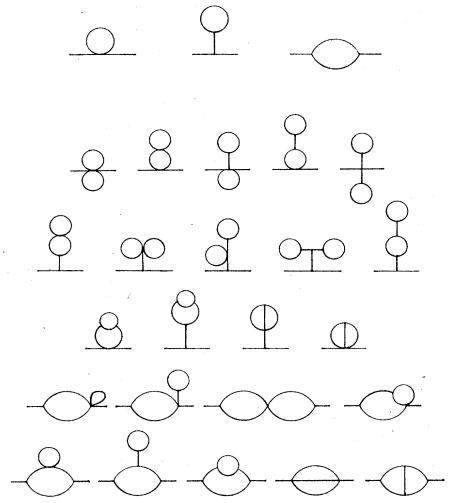

FIG. 5. One- and two-loop in-plane SC diagrams.

$$\begin{aligned}\omega=\omega^*[1&+\tfrac{1}{2}(\theta_{\Psi\Psi}^{(1)}+\theta_{SS}^{(1)}-2\theta_{\Psi S}^{(1)})\\&+\tfrac{1}{2}(\theta_{\Psi\Psi}^{(2)}+\theta_{SS}^{(2)}-2\theta_{\Psi S}^{(2)})\\&-\tfrac{1}{2}\theta_{\Psi S}^{(1)}(\theta_{\Psi\Psi}^{(1)}+\theta_{SS}^{(1)}-2\theta_{\Psi S}^{(1)})\\&-\tfrac{1}{8}(\theta_{\Psi\Psi}^{(1)}-\theta_{SS}^{(1)})^2]\ .\end{aligned} \tag{4.19}$$

The first-order correction is due only to one-loop graphs, while the second-order correction results from the two-loop graphs and products of the θ's of one-loop graphs. By the two-loop mass renormalization, we mean the entire second-order expansion (4.19). With this definition of one- and two-loop renormalization, we indeed find (as explained in the Introduction) that, as δ tends to zero, the renormalization vanishes separately in each order. The one-loop renormalization is less than 0.005 for $\delta<10^{-5}$ (and fields $2\ \mathrm{T}<H<10\ \mathrm{T}$). The two-loop graphs are much more difficult to compute numerically, especially as $\delta\to 0$, since some are more than logarithmically divergent with δ. However, we have seen that the two-loop correction decreases smoothly to less than 0.01 as δ decreases down to 10^{-4}.

V. RESULTS

We have calculated the renormalized magnon mass (i.e., the energy of the $q=0$ magnon) to the two-loop level as a function of external field and anisotropy parameter δ. Figure 6 shows the results for TMMC along with the unrenormalized mass, the SG results (3.11), and the experimental data.[13,14] (Figure 6 uses the best-fit values $J/k_B=13.1$ K and $\delta=0.019$, found by matching the two-loop calculation to the measured magnon energies at $k=\pi/2$ and π.[19]) Experimentally the zero-momentum renormalization is quite small, but the SG approximation results in a substantial change. The SC calculation, by including out-of-plane graphs neglected by the SG approximation, predicts a small renormalization, in close agree-

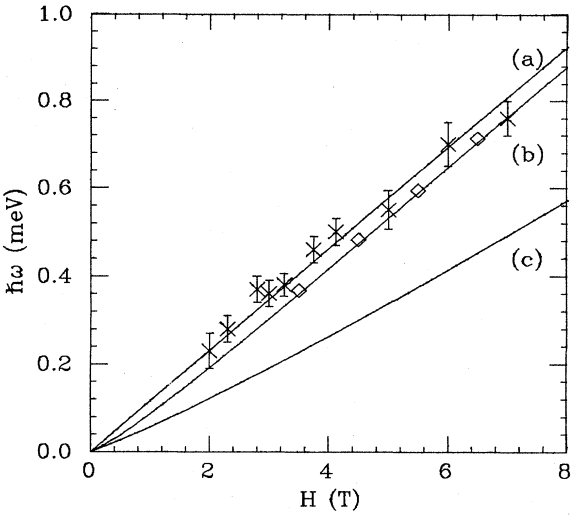

FIG. 6. Magnon mass as a function of field. The experimental results are taken from Ref. 13, denoted with ×, and the more recent data from Ref. 14, denoted with diamonds. The theoretical curves are (a) the harmonic SC [Eq. (4.7)], (b) the two-loop SC renormalized mass [Eq. (4.19)], (c) the two-loop SG renormalized mass [Eq. (3.11)].

ment with experiment. In this section we compare the SC and SG results in more depth, with an expectation of understanding when the latter is valid (as far as a description of the magnon energy is concerned). We also briefly discuss the accuracy of the two-loop calculation.

It is convenient to distinguish between diagrams that diverge with the cutoff Λ and those which remain finite. Of course for a real system the cutoff is fixed by the lattice spacing and there is no actual divergence. Nonetheless, in the limit of a small field ($\alpha \to 0$), the renormalization is dominated by the "divergent" graphs. In the SC, divergent in-plane diagrams [even the simple one-loop vacuum fluctuation graph in Fig. 4(a)] also have finite pieces, due to the momentum dependence of the interaction vertices. We can show that in the SG limit ($\alpha \to 0$) the divergent parts of the SC in-plane diagrams reproduce the divergent SG diagrams, through two loops in both theories. Thus the SG approximation is accurate when the out-of-plane SC graphs and the momentum-dependent finite parts of the in-plane graphs can be neglected.

As one would expect, the in-plane diagrams dominate when the motion is predominantly planar. It is easy to show [from (4.2), (4.4), and (4.5)] that in the harmonic approximation $\langle \Psi^2 \rangle \sim \ln(\pi/\alpha)$ and

$$\langle (S^z)^2 \rangle / S(S+1) \sim \ln(\pi/\sqrt{\delta}) \ .$$

The relative size of these zero-point motions is controlled by the ratio of the in-plane ($p=0$) to the out-of-plane ($p=\pi$) energy gaps, which, from Eq. (4.7), is proportional to $\alpha/\sqrt{\delta}$. In the case $\alpha \ll \sqrt{\delta}$ the spins are predominantly in the easy plane, and the in-plane graphs dominate. [For the SC system to be truly SG-like, and not merely planar, one also needs $\ln(\pi/\alpha) \gg 1$ so that the momentum-dependent finite parts of the SC in-plane graphs can be neglected.]

Figure 7 shows the one-loop downward renormalization

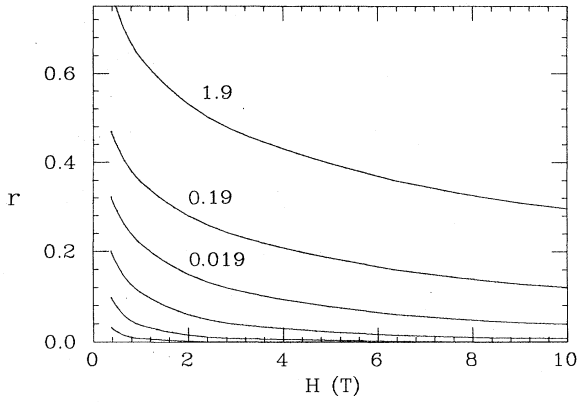

FIG. 7. One-loop SC downward renormalization of the magnon mass as a function of field, for curves of fixed δ. The bottom three curves are for the values $\delta=0.0019$, $\delta=0.000\,19$, and $\delta=0.000\,019$. The renormalized mass is $m=(1-r)m_0$.

of the magnon mass as a function of field for several values of δ. For any δ, as H decreases, the renormalization increases as the SG-like terms grow. However, for any value of H, the smaller δ, the smaller the renormalization. As explained in the Introduction, this symmetry must appear order by order in the loop expansion and indeed as δ tends to zero the first-order mass renormalization vanishes. For $\delta \sim 10^{-5}$, the one-loop renormalization is less than 0.005 for $2\ \mathrm{T} < H < 10\ \mathrm{T}$. For δ smaller than 0.1, the renormalizations resemble the isotropic $\delta=0$ limit much more than the planar (large-δ) limit. Figure 8 emphasizes the universality of small-δ behavior by plotting the one-loop renormalization against the mass gap ratio ω_0/ω_π. Curves for $\delta < 0.019$ lie on top of the $\delta=0.019$ curve. From Fig. 8 we also see that an in-plane approximation is quite good for large δ (e.g., $\delta=1.9$), but is very unsatisfactory for the TMMC value $\delta=0.019$.

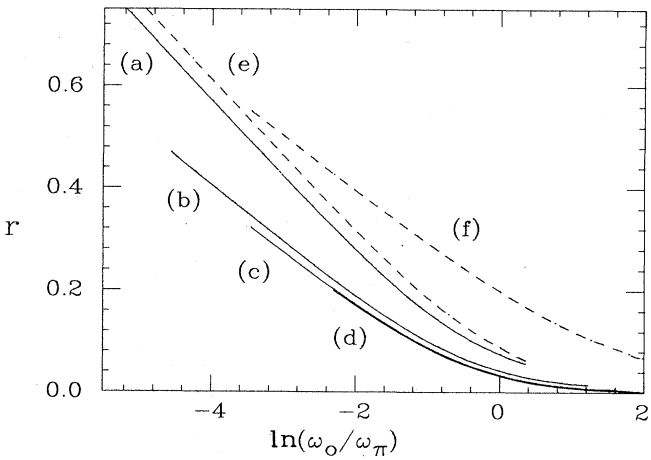

FIG. 8. One-loop downward renormalization of the SC magnon mass as a function of the gap ratio ω_0/ω_π (solid lines): (a) $\delta=1.9$, (b) $\delta=0.19$, (c) $\delta=0.019$ (TMMC), (d) $\delta=0.0019$, 0.000 19, and 0.000 019. In-plane downward renormalization (dashed lines) (e) $\delta=1.9$, (f) $\delta=0.019$ (TMMC).

The good agreement evident in Fig. 6 between experiment and the SC analysis applied to TMMC is due to the almost total cancellation of in-plane graphs by out-of-plane graphs. For example, in a field of 5 T, the two-loop in-plane renormalization is 28%, while including the out-of-plane diagrams reduces the correction to 8%. The presence of significant out-of-plane motion explains the deviation of the TMMC magnon mass from the prediction of the planar SG model. As explained in the Introduction, this cancellation must occur for systems (such as TMMC) which are near the isotropic limit.

Finally, we comment on the accuracy of the two-loop calculation as applied to TMMC. In the SG theory, keeping divergent terms (as defined above) to two loops is an excellent approximation to the infinite-order renormalization which results from normal ordering. (For TMMC at $H=5$ T, the corrections are, respectively, 40.6% and 40.5%.) One might hope for similar convergence for the SC theory, which adds out-of-plane corrections to the SG. Moreover, TMMC is very close to the isotropic $\delta=0$ limit. Since the isotropic symmetry is barely broken in TMMC, order by order in the SC loop expansion the renormalization must be small. Although some individual two-loop diagrams are quite large (θ up to 0.4), there are significant cancellations within each subset of graphs. In the end, the two-loop contribution to the renormalization is indeed small for TMMC. For example, at $H=5$ T, the one-loop renormalization is 7.8% and the second-order correction adds only an extra 0.2%. The two-loop correction remains small over the usual range of fields, so we believe the two-loop mass renormalization is quite accurate.

ACKNOWLEDGMENTS

We are indebted to Jim McCarthy and co-workers for the use of their computational facilities. We wish to thank Kazumi Maki for pointing out that certain two-loop graphs were omitted in an earlier version of this work. This work was supported by the National Science Foundation under Grant No. DMR-84-04955.

APPENDIX A

The expansion (2.7), continued to order $[S^z/\sqrt{S(S+1)}]^{-6}$, is written

$$\begin{aligned}\mathcal{H}=JS(S+1)\sum_{n=1}^{N}\Bigg[&\cos(\phi_n-\phi_{n+1})-4\sin(\alpha)\cos(\phi_n)+\frac{S_n^zS_{n+1}^z}{S(S+1)}\\&-\frac{1}{2}\frac{S_n^z}{\sqrt{S(S+1)}}[\cos(\phi_n-\phi_{n+1})+\cos(\phi_{n-1}-\phi_n)-4\sin(\alpha)\cos(\phi_n)-2\delta]\frac{S_n^z}{\sqrt{S(S+1)}}\\&-\frac{1}{8}\left[\frac{S_n^z}{\sqrt{S(S+1)}}\right]^2[\cos(\phi_n-\phi_{n+1})+\cos(\phi_{n-1}-\phi_n)-4\sin(\alpha)\cos(\phi_n)]\left[\frac{S_n^z}{\sqrt{S(S+1)}}\right]^2\\&+\frac{1}{4}\frac{S_n^zS_{n+1}^z}{S(S+1)}\cos(\phi_n-\phi_{n+1})\frac{S_n^zS_{n+1}^z}{S(S+1)}\\&-\frac{1}{16}\left[\frac{S_n^z}{\sqrt{S(S+1)}}\right]^3[\cos(\phi_n-\phi_{n+1})+\cos(\phi_{n-1}-\phi_n)-4\sin(\alpha)\cos(\phi_n)]\left[\frac{S_n^z}{\sqrt{S(S+1)}}\right]^3\\&+\frac{1}{16}\frac{(S_n^z)^2S_{n+1}^z}{[\sqrt{S(S+1)}]^3}[\cos(\phi_n-\phi_{n+1})+\cos(\phi_{n-1}-\phi_n)]\frac{(S_n^z)^2S_{n+1}^z}{[\sqrt{S(S+1)}]^3}\\&+O\left[\left[\frac{S_n^z}{\sqrt{S(S+1)}}\right]^8\right]\Bigg].\end{aligned}\tag{A1}$$

Using the change of variables (2.9), and transforming to momentum space (4.2), we write

$$\mathcal{H}=\mathcal{H}_0+\mathcal{H}',\tag{A2}$$

where $\mathcal{H}_0$ is the quadratic term given in (4.3), and

$$\mathcal{H}'=\mathcal{H}_3+\mathcal{H}_4+\mathcal{H}_5+\mathcal{H}_6+\cdots.\tag{A3}$$

In the following, we use the notation

$$q=q_1+q_2+q_3+\cdots+q_m \text{ within } \mathcal{H}_m.\tag{A4}$$

The terms in (A3) are

$$\mathscr{H}_3=-JS(S+1)\sin(2\alpha)\frac{1}{\sqrt{N}}\sum_{q_1,q_2,q_3}\delta_{q,\pm\pi}\left\{\tfrac{1}{3}[1+4e^{i(q-\pi)/2}\sin(\tfrac{1}{2}q_1)\sin(\tfrac{1}{2}q_2)\sin(\tfrac{1}{2}q_3)]\Psi_{q_1}\Psi_{q_2}\Psi_{q_3}\right.$$
$$\left.+\cos(q_2)\frac{S^z_{q_1}\Psi_{q_2}S^z_{q_3}}{S(S+1)}\right\}, \tag{A5}$$

$$\mathscr{H}_4=-JS(S+1)\frac{1}{N}\sum_{q_1,q_2,q_3,q_4}\delta_{q,0}\left\{\tfrac{1}{6}[\sin^2\alpha+4\cos(2\alpha)\sin(\tfrac{1}{2}q_1)\sin(\tfrac{1}{2}q_2)\sin(\tfrac{1}{2}q_3)\sin(\tfrac{1}{2}q_4)]\Psi_{q_1}\Psi_{q_2}\Psi_{q_3}\Psi_{q_4}\right.$$
$$+\{\sin^2\alpha-2\cos(2\alpha)\sin(\tfrac{1}{2}q_2)\sin(\tfrac{1}{2}q_3)\cos[\tfrac{1}{2}(q_1+q_4)]\}\frac{S^z_{q_1}\Psi_{q_2}\Psi_{q_3}S^z_{q_4}}{S(S+1)}$$
$$-\tfrac{1}{12}\{3-\cos(2\alpha)[\cos(q_1+q_2)+\cos(q_1+q_3)+\cos(q_2+q_3)]\}$$
$$\left.\times\frac{S^z_{q_1}S^z_{q_2}S^z_{q_3}S^z_{q_4}}{S^2(S+1)^2}\right\}, \tag{A6}$$

$$\mathscr{H}_5=JS(S+1)\sin(2\alpha)\frac{1}{N^{3/2}}$$
$$\times\sum_{q_1,q_2,\ldots,q_5}\delta_{q,\pm\pi}\left\{\tfrac{1}{60}[1-16e^{i(q-\pi)/2}\sin(\tfrac{1}{2}q_1)\sin(\tfrac{1}{2}q_2)\times\cdots\times\sin(\tfrac{1}{2}q_5)]\Psi_{q_1}\Psi_{q_2}\Psi_{q_3}\Psi_{q_4}\Psi_{q_5}\right.$$
$$+\tfrac{1}{6}\{1+8e^{i(q-\pi)/2}\sin(\tfrac{1}{2}q_2)\sin(\tfrac{1}{2}q_3)\sin(\tfrac{1}{2}q_4)\cos[\tfrac{1}{2}(q_1+q_5)]\}\frac{S^z_{q_1}\Psi_{q_2}\Psi_{q_3}\Psi_{q_4}S^z_{q_5}}{S(S+1)}$$
$$\left.-\tfrac{1}{8}[2\cos(q_3)+\cos(q_1+q_4)+\cos(q_1+q_5)+\cos(q_2+q_4)+\cos(q_2+q_5)]\frac{S^z_{q_1}S^z_{q_2}\Psi_{q_3}S^z_{q_4}S^z_{q_5}}{S^2(S+1)^2}\right\}, \tag{A7}$$

$$\mathscr{H}_6=JS(S+1)\frac{1}{N^2}$$
$$\times\sum_{q_1,\ldots,q_6}\delta_{q,0}\left\{\tfrac{1}{180}[\sin^2\alpha-16\cos(2\alpha)\sin(\tfrac{1}{2}q_1)\sin(\tfrac{1}{2}q_2)\times\cdots\times\sin(\tfrac{1}{2}q_6)]\Psi_{q_1}\Psi_{q_2}\times\cdots\times\Psi_{q_6}\right.$$
$$+\tfrac{1}{12}\{\sin^2\alpha+8\cos(2\alpha)\sin(\tfrac{1}{2}q_2)\sin(\tfrac{1}{2}q_3)\sin(\tfrac{1}{2}q_4)\sin(\tfrac{1}{2}q_5)\cos[\tfrac{1}{2}(q_1+q_6)]\}\frac{S^z_{q_1}\Psi_{q_2}\Psi_{q_3}\Psi_{q_4}\Psi_{q_5}S^z_{q_6}}{S(S+1)}$$
$$-\tfrac{1}{4}\{\sin^2\alpha+2\cos(2\alpha)\sin(\tfrac{1}{2}q_3)\sin(\tfrac{1}{2}q_4)\cos[\tfrac{1}{2}(q_1-q_2)]\cos[\tfrac{1}{2}(q_5-q_6)]$$
$$+2\cos(2\alpha)\sin(\tfrac{1}{2}q_3)\sin(\tfrac{1}{2}q_4)\cos[\tfrac{1}{2}(q_3+q_4)]\}\frac{S^z_{q_1}S^z_{q_2}\Psi_{q_3}\Psi_{q_4}S^z_{q_5}S^z_{q_6}}{S^2(S+1)^2}$$
$$+\frac{1}{120}\left[15-\cos(2\alpha)\sum_{\substack{i\neq j\\ i=1}}^{6}\cos(q_i+q_j)\right]\left.\frac{S^z_{q_1}S^z_{q_2}S^z_{q_3}S^z_{q_4}S^z_{q_5}S^z_{q_6}}{S^3(S+1)^3}\right\}. \tag{A8}$$

APPENDIX B

Define the zero-temperature magnon Green's-function matrix using Eqs. (4.8) and (4.9). In this appendix we show that, if S^z and Ψ are canonical variables, a matrix form of Dyson's equation holds true:

$$[\underline{D}(p,\omega)]^{-1}=[\underline{D}^0(p,\omega)]^{-1}-\underline{\Sigma}(p,\omega)\ , \tag{B1}$$

where $\underline{D}^0$ is the free propagator matrix and $\underline{\Sigma}$, the self-energy matrix, is the sum of the irreducible vertex parts as defined below. The proof closely follows the ordinary development.[22]

We expand each element of $\underline{D}$ in the usual perturbation series:

$$D_{\mu\nu}(p,t-t')=\sum_{n=0}^{\infty}\frac{(-i)^{n+1}}{n!}\int_{-\infty}^{\infty}dt_1\int_{-\infty}^{\infty}dt_2\cdots\int_{-\infty}^{\infty}dt_n\langle T[\Phi_p^{\mu}(t)\Phi_{-p}^{\nu}(t')\mathscr{H}'(t_1)\mathscr{H}'(t_2)\times\cdots\times\mathscr{H}'(t_n)]\rangle_{\text{conn}}\ , \tag{B2}$$

where $\langle\ \rangle_{\text{conn}}$ means only the connected graphs are included in Wick's expansion of the bracket.

Consider again the form of $n=1$ contribution of $\mathscr{H}_4^b$ to (B2) [Eq. (4.16)]:

$$D_{\Psi\Psi}^{(4b)}(p,\omega)=D_{\Psi\Psi}^0\Sigma_{\Psi\Psi}^{(4b)}D_{\Psi\Psi}^0+D_{\Psi S}^0\Sigma_{SS}^{(4b)}D_{S\Psi}^0+D_{\Psi S}^0\Sigma_{\Psi S}^{(4b)}D_{S\Psi}^0+D_{\Psi S}^0\Sigma_{S\Psi}^{(4b)}D_{\Psi\Psi}^0\ . \tag{B3}$$

In our notation $D_{\mu\nu}^0$ is the free propagator and $\Sigma_{\mu\nu}^{(4b)}$ are the self-energy parts, the graphs with the initial and final propagators factored out. The subscripts μ and ν in $\Sigma_{\mu\nu}$ mean the entry and exit operators are Φ^{μ} and Φ^{ν}, respectively. The notation of (B3) is suggestive: $D_{\Psi\Psi}^{(4b)}(p,\omega)$ is the (Ψ,Ψ) component of a matrix

$$\underline{D}^{(4b)}(p,\omega)=\underline{D}^0\underline{\Sigma}^{(4b)}\underline{D}^0\ , \tag{B4}$$

and in fact it is easy to see that this gives the correct $n=1$ contribution for each $D_{\mu\nu}$ in Eq. (B2). If we define $\Sigma_{\mu\nu}^{(1)}$ to be the sum of all the $n=1$ self-energy parts with entry (exit) operator Φ^{μ} (Φ^{ν}), then an equation such as (B4) gives the total $n=1$ contribution.

For n arbitrary, $D^{(n)}$ consists of all graphs with n vertices. Note first that each graph represents $n!$ equal terms in the Wick's expansion of $\langle\ \rangle_{\text{conn}}$, terms which differ only in the rearrangement of the t_i, so that the permutations of $t_1,t_2,\ldots,t_n$ cancel the $1/n!$ in Eq. (B2).

The higher-order graphs ($n>1$) are either reducible (separable into two lower-order graphs by cutting a single line) or irreducible. Consider the irreducible graphs. Exactly as in the $n=1$ case, the contribution to $D_{\mu\nu}^{(n)}$ of an nth-order irreducible graph with entry (exit) operator $\Phi^{\mu'}$ ($\Phi^{\nu'}$) can be written

$$D_{\mu\nu}^{(n)}(q,\omega)=D_{\mu\mu'}^0\Sigma_{\mu'\nu'}^{(n)}D_{\nu'\nu}^0\ . \tag{B5}$$

$\Sigma_{\mu'\nu'}^{(n)}$ is the "self-energy part" of the graph and includes a factor $(-i)^{n-1}$ from (B2). Define $N_{\mu\nu}^n$ to be the number of irreducible graphs of order n, with entry (exit) operator Φ^{μ} (Φ^{ν}) obtained in the Wick's expansion of Eq. (B2). We will label these self-energy parts $\Sigma_{\mu\nu}^{(n,j)}$, $j=1,2,\ldots,N_{\mu\nu}^n$. If we define $\Sigma_{\mu\nu}^{(n)}$ to be the sum of the irreducible self-energy parts,

$$\Sigma_{\mu\nu}^{(n)}=\sum_{j=1}^{N_{\mu\nu}^n}\Sigma_{\mu\nu}^{(n,j)}\ , \tag{B6}$$

then the contribution of all the nth-order irreducible graphs to $D^{(n)}$ is

$$\underline{D}_{\text{irred}}^{(n)}(p,\omega)=\underline{D}^0\underline{\Sigma}^{(n)}\underline{D}^0\ . \tag{B7}$$

Finally, consider the entire term $\underline{D}^{(n)}$, including reducible diagrams. $D_{\mu\nu}^{(n)}$ is the sum of all terms of the form

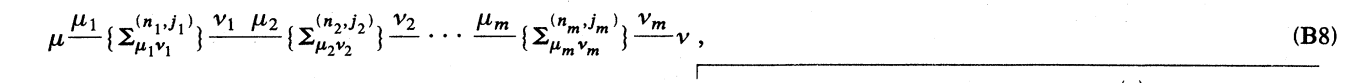

(B8)

where

$$n_1+n_2+\cdots+n_m=n\ , \tag{B9}$$

so that the graph is nth order. The ith term (in curly brackets) above consists of the (j_ith) irreducible graph of order n_i, with entry (exit) operator Φ^{μ} (Φ^{ν}). The above diagram represents the following contribution to $D^{(n)}$:

$$D_{\mu\nu}^{(n)}(p,\omega)=D_{\mu\mu_1}^0\Sigma_{\mu_1\nu_1}^{(n_1,j_1)}D_{\nu_1\mu_2}^0\Sigma_{\mu_2\nu_2}^{(n_2,j_2}\times\cdots\times\Sigma_{\mu_m\nu_m}^{(n_m,j_m)}D_{\nu_m\nu}^0\ . \tag{B10}$$

[Note that the $m+1$ lines in the above figure each absorb a factor $(-i)$, and a self-energy part $\Sigma^{(r)}$ absorbs $(-i)^{r-1}$, so that the $(-i)^{n+1}$ in (B2) is used up.]

The total nth order contribution $D^{(n)}$ is the sum of all such graphs; that is, including every possible choice of m and arrangement $\{n_i,j_i\}$, and then summing over each choice of μ_i,ν_i. Using (B6) we find that the total nth-order contribution is

$$\underline{D}^{(n)}(p,\omega)=\sum_{m,\{n_i\}}\underline{D}^0\underline{\Sigma}^{(n_1)}\underline{D}^0\underline{\Sigma}^{(n_2)}\times\cdots\times\Sigma^{(n_m)}\underline{D}^0\ , \tag{B11}$$

where the sum is over all $m,\{n_i\}$ satisfying (B9).

The total Green's function is the sum of (B11) over all n, or equivalently, the sum of all graphs like diagram (B8) with any choice of $m,\{n_i\}$. This gives

$$\underline{D}(p,\omega)=\underline{D}^0+\sum_{m=1}^{\infty}\sum_{n_i=1}^{\infty}\underline{D}^0\underline{\Sigma}^{(n_1)}\underline{D}^0\underline{\Sigma}^{(n_2)}\times\cdots\times\underline{\Sigma}^{(n_m)}\underline{D}^0\ . \tag{B12}$$

Finally, define the self-energy matrix as the sum of all the irreducible self-energy parts:

$$\underline{\Sigma}=\sum_{n=1}^{\infty}\underline{\Sigma}^{(n)}\,. \tag{B13}$$

Then (B12) becomes

$$\underline{D}=\underline{D}^0+\sum_{m=1}^{\infty}\underline{D}^0\underline{\Sigma}\underline{D}^0\underline{\Sigma}\times\cdots\times\underline{\Sigma}\underline{D}^0 \quad (m \text{ factors of } \underline{\Sigma}) \tag{B14}$$

$$=\underline{D}^0(1+\underline{D}^0\underline{\Sigma}+\underline{D}^0\underline{\Sigma}\underline{D}^0\underline{\Sigma}+\cdots)\,. \tag{B15}$$

We formally sum (B15) to obtain (B1).

The analytic structure of $\underline{D}(q,\omega)$ in the ω plane is due solely to the denominator of (4.11). A pole in, say, θ_{SS} in the numerator is cancelled by θ_{SS} in the denominator.

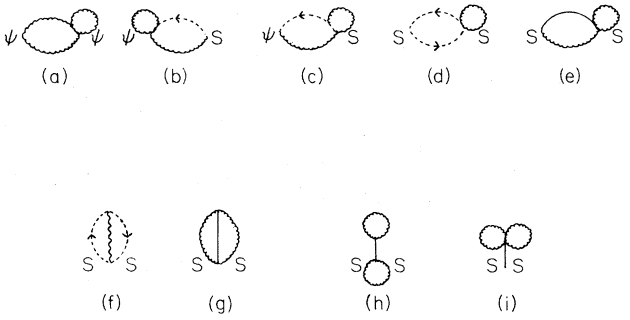

FIG. 9. Diagrams of the $n=2$ graphs from $\{\mathscr{H}_3^{\rm b},\mathscr{H}_5^{\rm c}\}$, evaluated in Appendix C.

APPENDIX C

As a further example of the graphical technique applied to the spin-chain Hamiltonian, we compute the $n=2$ contributions to the Σ functions arising from the cross terms $\mathscr{H}_3^{\rm b},\mathscr{H}_5^{\rm c}$ in the expansion (4.13):

$$D_{\mu\nu}^{3{\rm b},5{\rm c}}(p,t-t')=(-i)^3\int_{-\infty}^{\infty}dt_1\int_{-\infty}^{\infty}dt_2\langle T[\Phi_p^{\mu}(t)\phi_{-p}^{\nu}(t')\mathscr{H}_3^{\rm b}(t_1)\mathscr{H}_5^{\rm c}(t_2)]\rangle_{\rm conn}\,. \tag{C1}$$

From the expansion of $\mathscr{H}'$ in Appendix A, we obtain

$$D_{\mu\nu}^{3{\rm b},5{\rm c}}(p,\omega)=(-i)^3\int_{-\infty}^{\infty}d(t-t')e^{i\omega(t-t')}\int_{-\infty}^{\infty}dt_1\int_{-\infty}^{\infty}dt_2\sum_{q,k}V_3^{\rm b}(\mathbf{q})V_5^{\rm c}(\mathbf{k})$$
$$\times\langle T[\phi_p^{\mu}(t)\phi_{-p}^{\nu}(t')\{S_{q_1}^z\Psi_{q_2}S_{q_3}^z\}(t_1)\{S_{k_1}^zS_{k_2}^z\Psi_{k_3}S_{k_4}^zS_{k_5}^z\}(t_2)]\rangle\,. \tag{C2}$$

From the Wick's expansion of (C2) we obtain the noncancelling graphs drawn in Fig. 9. The graphs in Figs. 9(a)–9(e) are dependent upon ω; those in Figs. 9(f)–9(i) are not. Using the notation $q'=\pi+p-q$, their contributions to the Σ functions are as follows:

$$\Sigma_{\Psi\Psi}^{(a)}(p,\omega)=-\frac{4J^2\sin^2(2\alpha)}{S(S+1)}\frac{1}{(2\pi)^2}\int_{-\pi}^{\pi}dq\int_{-\pi}^{\pi}dk\,\beta_q^2\beta_{q'}^2\beta_k^2\frac{\omega_q+\omega_{q'}}{(\omega_q+\omega_{q'})^2-\omega^2-i\epsilon}$$
$$\times\cos(p)\{1+2\cos(p)+2\cos(k)[\cos(q)+\cos(q')]\}\,, \tag{C3}$$

$$\Sigma_{\Psi S}^{(b)}(p,\omega)=-\frac{2J^2\sin^2(2\alpha)}{S(S+1)}\frac{1}{(2\pi)^2}\int_{-\pi}^{\pi}dq\int_{-\pi}^{\pi}dk\,\beta_q^2\beta_k^2\frac{-i\omega}{(\omega_q+\omega_{q'})^2-\omega^2-i\epsilon}$$
$$\times\cos(q')\{1+2\cos(p)+2\cos(k)[\cos(q)+\cos(q')]\}\,, \tag{C4}$$

$$\Sigma_{\Psi S}^{(c)}(p,\omega)=-\frac{2J^2\sin^2(2\alpha)}{S(S+1)}\frac{1}{(2\pi)^2}\int_{-\pi}^{\pi}dq\int_{-\pi}^{\pi}dk\,\beta_q^2\beta_k^2\frac{-i\omega}{(\omega_q+\omega_{q'})^2-\omega^2-i\epsilon}$$
$$\times\cos(p)\{1+2\cos(q')+2\cos(k)[\cos(p)+\cos(q)]\}\,, \tag{C5}$$

$$\Sigma_{SS}^{(d)}(p,\omega)=-\frac{2J^2\sin^2(2\alpha)}{S(S+1)}\frac{1}{(2\pi)^2}\int_{-\pi}^{\pi}dq\int_{-\pi}^{\pi}dk\,\beta_k^2\frac{\omega_q+\omega_{q'}}{(\omega_q+\omega_{q'})^2-\omega^2-i\epsilon}$$
$$\times\cos(q)\{1+2\cos(q')+2\cos(k)[\cos(p)+\cos(q)]\}\,, \tag{C6}$$

$$\Sigma_{SS}^{(e)}(p,\omega)=-\frac{8J^2\sin^2(2\alpha)}{S(S+1)}\frac{1}{(2\pi)^2}\int_{-\pi}^{\pi}dq\int_{-\pi}^{\pi}dk\,\alpha_q^2\beta_{q'}^2\beta_k^2\frac{\omega_q+\omega_{q'}}{(\omega_q+\omega_{q'})^2-\omega^2-i\epsilon}$$
$$\times\cos(q)\{1+2\cos(q)+2\cos(k)[\cos(p)+\cos(q')]\}\,. \tag{C7}$$

With the notation $q_1+q_2+q_3=\pi$ we write

$$\Sigma_{SS}^{(f)}(p,\omega)=-\frac{2J^2\sin^2(2\alpha)}{S(S+1)}\frac{1}{(2\pi)^2}\int_{-\pi}^{\pi}dq_1\int_{-\pi}^{\pi}dq_2\,\beta_{q_3}^2\frac{1}{\omega_{q_1}+\omega_{q_2}+\omega_{q_3}}$$
$$\times\cos(q_2)\{1+2\cos(q_1)+2\cos(p)[\cos(q_2)+\cos(q_3)]\}\,, \tag{C8}$$

$$\Sigma_{SS}^{(g)}(p,\omega)=-\frac{4J^2\sin^2(2\alpha)}{S(S+1)}\frac{1}{(2\pi)^2}\int_{-\pi}^{\pi}dq_1\int_{-\pi}^{\pi}dq_2\,\alpha_{q_1}^2\beta_{q_2}^2\beta_{q_3}^2\frac{1}{\omega_{q_1}+\omega_{q_2}+\omega_{q_3}}$$
$$\times\cos(q_1)\{1+2\cos(q_1)+2\cos(p)[\cos(q_2)+\cos(q_3)]\}\,, \tag{C9}$$

$$\Sigma_{SS}^{(h)}(p,\omega)=-\frac{J\sin^2(\alpha)}{[S(S+1)]^2(2\pi)^2}\int_{-\pi}^{\pi}dq\int_{-\pi}^{\pi}dk\,\beta_q^2\beta_k^2[1-4\cos(p)\cos(q)]\,, \tag{C10}$$

$$\Sigma_{SS}^{(i)}(p,\omega)=-\frac{J\sin^2(\alpha)}{2[S(S+1)]^2(2\pi)^2}\int_{-\pi}^{\pi}dq\int_{-\pi}^{\pi}dk\,\beta_q^2\beta_k^2[1-4\cos(k)\cos(q)]\,. \tag{C11}$$

[1]K. M. Leung, D. W. Hone, D. L. Mills, P. S. Riseborough, and S. E. Trullinger, Phys. Rev. B **21**, 4017 (1980).

[2]H. J. Mikeska, J. Phys. C **13**, 2913 (1980).

[3]H. J. Mikeska, J. Appl. Phys. **52**, 1950 (1981).

[4]K. Maki, Phys. Rev. B **24**, 3991 (1981).

[5]K. Maki, in *Progress in Low Temperature Physics,* edited by D. F. Brewer (North-Holland, Amsterdam, 1982), Vol. VIII.

[6]F. Borsa, Phys. Rev. B **25**, 3430 (1982).

[7]F. Borsa, M. G. Pini, A. Rettori, and V. Tognetti, Phys. Rev. B **28**, 5173 (1983).

[8]K. Sasaki and T. Tsuzuki, J. Magn. Magn. Mater. **31-34**, 1283 (1983).

[9]M. Steiner, J. Magn. Magn. Mater. **31-34**, 1277 (1983).

[10]X. Zotos, J. Phys. (Paris) Colloq. **44**, C3-477 (1983).

[11]A summary of some of this work previously appeared in M. Fowler, N. F. Wright, and M. D. Johnson, in *Magnetic Excitations and Fluctuations,* edited by S. W. Lovesey, U. Balucani, F. Borsa, and V. Tognetti (Springer, Heidelberg, 1984), p. 99.

[12]M. Steiner, J. Villain, and C. G. Windsor, Adv. Phys. **25**, 87 (1976).

[13]I. U. Heilmann, J. K. Kjems, Y. Endoh, G. F. Reiter, G. Shirane, and R. J. Birgeneau, Phys. Rev. B **24**, 3939 (1981).

[14]The most recent results are in Y. Endoh, Y. Ajiro, H. Shiba, and H. Yoshizawa, Phys. Rev. B **30**, 4074 (1984). We would like to thank H. Shiba for bringing these results to our attention after we had completed the work presented here.

[15]P. S. Riseborough and G. F. Reiter, Phys. Rev. B **27**, 1844 (1983).

[16]E. S. Abers and B. W. Lee, Phys. Rep. **9C**, 1 (1973).

[17]F. D. M. Haldane, Phys. Lett. **93A**, 464 (1983).

[18]K. Maki and H. Takayama, Phys. Rev. B **20**, 3223 (1979).

[19]K. Osano, H. Shiba, and Y. Endoh, Prog. Theor. Phys. **67**, 995 (1982).

[20]P. Carruthers and M. M. Nieto, Rev. Mod. Phys. **40**, 411 (1968).

[21]S. Coleman, Phys. Rev. D **15**, 2088 (1975).

[22]A. A. Abrikosov, L. P. Gor'kov, and I. E. Dzyaloshinskii, *Methods of Quantum Field Theory in Statistical Physics* (Prentice-Hall, Englewood Cliffs, 1963).